

Distribution Agreement

In presenting this thesis as a partial fulfillment of the requirements for a degree from Emory University, I hereby grant to Emory University and its agents the non-exclusive license to archive, make accessible, and display my thesis in whole or in part in all forms of media, now or hereafter now, including display on the World Wide Web. I understand that I may select some access restrictions as part of the online submission of this thesis. I retain all ownership rights to the copyright of the thesis. I also retain the right to use in future works (such as articles or books) all or part of this thesis.

Ally Jane Su

April 27, 2022

A Novel Diagnostic Assay for Platelet-Type von Willebrand Disease

by

Ally Jane Su

Renhao Li
Adviser

Chemistry Department

Renhao Li
Adviser

Vincent Conticello
Committee Member

Antonio Brathwaite
Committee Member

2022

A Novel Diagnostic Assay for Platelet-Type von Willebrand Disease

By

Ally Jane Su

Renhao Li

Adviser

An abstract of
a thesis submitted to the Faculty of Emory College of Arts and Sciences
of Emory University in partial fulfillment
of the requirements of the degree of
Bachelor of Science with Honors

Chemistry

2022

Abstract

A Novel Diagnostic Assay for Platelet-Type von Willebrand Disease

By Ally Jane Su

Platelet-type von Willebrand disease (PT-VWD) is rare and often misdiagnosed due to its phenotypically similar symptoms with type 2B VWD. Both subtypes possess gain-of-function mutations that increase the affinity between the von Willebrand factor (VWF) and the glycoprotein Ib α of the platelets. For PT-VWD, this mutation occurs on GPIb α . For type 2B VWD, it develops on VWF. The current diagnosis utilizes ristocetin-induced platelet aggregation mixed studies and genetic sequencing, which are unstandardized and expensive. This study established a cell-based model for PT-VWD to circumvent obtaining patient plasma samples and developed a flow cytometry assay to identify PT-VWD. A stable cell line expressing mutated GPIb α (W230L) was generated through transfection and maintained with hygromycin. GPIb α (W230L) bound to full-length VWF and monomeric A1 at a higher affinity than GPIb α WT, as observed in flow cytometry. The binding difference between GPIb α (W230L) and GPIb α WT was amplified in a dose-dependent manner when incubated with activators such as ristocetin and 1D12. Utilizing truncated A1 (NAIM-A1) or diluting plasma at a 1:1 ratio also heightened the binding difference between GPIb α (W230L) and GPIb α WT. By employing these parameters to maximize the binding of GPIb α (W230L), it becomes possible to identify PT-VWD and diagnose patients via a rapid and accessible assay.

A Novel Diagnostic Assay for Platelet-Type von Willebrand Disease

By

Ally Jane Su

Renhao Li

Adviser

A thesis submitted to the Faculty of Emory College of Arts and Sciences
of Emory University in partial fulfillment
of the requirements of the degree of
Bachelor of Science with Honors

Chemistry

2022

Acknowledgements

I like to thank my research advisor, Renhao Li, for his guidance through my three years of undergraduate research. He had pushed me to become a better scientist by critically thinking, asking questions, and becoming confident in my work. I would also like to thank my mentor, Nicholas Arce, for tirelessly answering all my questions and being a role model.

I like to thank my committee members, Vincent Conticello and Antonio Brathwaite, for their support in my thesis work and for having the pleasure to take their undergraduate classes.

I like to thank my mother for igniting my passion for biochemistry at a young age. She had been a vital supporter of my journey as a scientist and loved learning about my research. Lastly, I would like to thank my boyfriend and friends for their encouragement throughout my thesis work.

Table of Contents

Chapter 1. An Introduction to von Willebrand Disease and von Willebrand Factor	1
1.1. An Overview	2
1.2. von Willebrand Disease	2
1.3. Glycoprotein Ib-IX	3
1.4. Platelet-Type von Willebrand Disease	3
1.4.1. Ristocetin-Induced Platelet Aggregation Mixed Studies	4
1.4.2. Genetic Testing	5
1.4.3. Issues	5
Chapter 2. Materials and Methods	6
2.1. Experimental Overview	7
2.2. Establishment of a Stable Cell Line	7
2.2.1. The Plasmid	7
2.2.2. Restriction Digestion	7
2.2.3. Cell Culture	8
2.2.4. Transfection	9
2.2.5. Cell Lysis	9
2.2.6. Western Blot	9
2.2.7. Cell Sorting	10
2.3. Flow Cytometry	10
2.3.1. Expression of GPIIb β and GPIX	11
2.3.2. GPIIb α Binding to Full-length VWF	11
2.4. Activators	11
2.5. Data analysis on FlowJo	12
Chapter 3. Results	13
3.1. Establishment of a Stable Cell Line	14
3.1.1. Confirming the plasmid with Restriction Digestion	14
3.1.2. Visualizing GFP in CHO cells	14
3.1.3. Checking the Success of the Transient transfection of GPIIb α	15
3.1.4. Flow cytometry	16
3.2. Higher Binding affinity of GPIIb α	17
3.3. Optimizing the conditions	17
3.3.1. GPIIb α (W230L) Responds Dose-Dependently to Botrocetin	18
3.3.2. GPIIb α (W230L) Exhibits Higher Binding to NAIM-A1 (1238-1461)	19
3.3.3. Determining the Ideal Plasma Concentration at a 1:1 Dilution	20
3.3.4. 1D12 is a Great Activator	
Chapter 4. Discussion	21
4.1. Optimizing the Use of Streptavidin-Conjugated Violet Fluorophore Beads	22
4.2. Further Studies with Ristocetin	24
4.3. The Declining Homogeneity of the CHO cell line	24
4.4. Conclusion	25

References

26

Figure 1

8

Figure 2

12

Figure 3

15

Figure 4

17

Figure 5

18

Figure 6

19

Figure 7

23

**Chapter 1. An Introduction to von Willebrand Factor and Platelet-Type Willebrand
Disease**

1.1 An Overview

von Willebrand factor (VWF) is a multimeric protein consisting of almost thirty different subunits in each monomer.¹⁻⁵ It possesses three A domains, A1,⁶⁻¹⁰ A2,¹¹⁻¹³ and A3,¹⁴⁻¹⁶ each contributing specific functions to the protein. The D assemblies bind to other proteins such as factor VIII, mediate assembly, and act as a site for disulfide linkages.^{3, 17} The VWC modules provide VWF with length and flexibility,¹⁸ and the O-glycosylated polypeptides contain the binding site to ristocetin.¹⁹⁻²¹ VWF is released in the bloodstream after being cleaved by ADAMTS13.²² Under normal conditions, VWF is coiled^{23, 24} and inactive. However, flow forces with varying velocities in the bloodstream called shear flow can occur during an injury.¹⁸ These forces cause VWF to become unwound.^{25, 26} The different subunits of VWF, including the A1 domain, are now exposed to their surrounding environment. Located from amino acids 1238 to 1493, the A1 domain contains the binding epitope for the glycoprotein (GP)Ib-IX complexes expressed on the surface of platelets.^{6, 10, 27} The A1 domain allows VWF to interact and bind with platelets.²⁸⁻³³ Containing up to 200 monomers,³⁴ VWF acts as a net that traps platelets to induce blood aggregation.

1.2 von Willebrand Disease

von Willebrand disease (VWD) is one of the most common genetic bleeding disorders in the United States that affects up to 1% of the population.³⁵ In healthy individuals, clots consisted of red blood cells and platelets will form at the site of blood vessel injuries to prevent further blood loss. In individuals with von Willebrand disease, clot formation does not occur normally. VWD is the broad term to describe diseases that arise from defected VWF. There are three main types of VWD—type 1, type 2, and type 3.⁴ Type 1 and type 3 are categorized as quantitative defects in VWF and type 2 as qualitative defects in VWF. Type 1 patients have lower-than-average VWF levels and can present symptoms of excessive

bleeding.³⁵ Patients with type 3 VWD also possess a quantitative defect in VWF; however, they have low levels of factor VIII in addition to low levels of VWF.³⁵ Factor VIII is a similar blood-clotting protein that binds to VWF to stabilize its half-life.¹⁸ Type 2 VWD is characterized by a qualitative defect in VWF and is categorized into four subtypes—2A, 2B, 2M, and 2N.³⁵ Specifically, type 2B VWD possesses a gain-of-function mutation located on the A1 domain to increase its binding affinity to GPIb α .³⁶

1.3. Glycoprotein Ib-IX

The glycoprotein (GP)Ib-IX receptor is one of the most common receptors expressed on the surface of platelets. The complex contains three distinct subunits, GPIb α , GPIb β , and GPIIX, expressed in a 1:2:1 ratio, respectively.^{37, 38} The GPIb α subunit is the largest among the three, containing seven leucine-rich repeats³⁹ and a “thumb” region responsible for binding to the A1 domain of VWF.^{37, 40} The negatively charged GPIb α interacts with the positively charged A1⁶. Even though GPIb α contains most of the bindings sites for the GPIb-IX complex, studies have observed that GPIb α will not be expressed if the surface lacked expression of GPIb β and GPIIX.⁴¹

1.4. Platelet-Type VWD

In 1980 and 1982, Takahashi and Miller almost simultaneously published their data on a puzzling new subtype of von Willebrand disease.^{42, 43} Despite patients producing identical symptoms of type 2B VWD, their von Willebrand factor demonstrated normal binding activity with platelets from a healthy individual.^{42, 43} On the other hand, when their platelets were exposed to von Willebrand factor from a healthy individual, the assay had demonstrated higher than normal levels of aggregation.^{42, 43} Miller coined the term “platelet-type von Willebrand disease”⁴² to describe this rare and unusual form of VWD in which a gain-of-function mutation on GPIb α induced higher binding affinity with VWF.^{4, 7} As a

result, the longer VWF concatemers were cleared selectively⁴⁴ and perceptible for cleavage by ADATMS13,¹⁸ resulting in symptoms of excessive bleeding.

Four mutations were reported to induce platelet-type (PT) VWD—W230L, G233V, M239V, and a 27 base pair deletion.⁴⁵ G233V is the most common mutation while W230L is the least common.⁴⁶ Interestingly, the W230L mutation exhibited the most detrimental effects by inducing the greatest increase of GPIIb/IIIa's binding to A1.⁴⁷ Studies have demonstrated through hydrogen-deuterium exchange that the mutations induce a conformational change which destabilizes GPIIb/IIIa^{6, 7, 48} and exposes its A1 binding site.^{47, 49}

Although type 2B VWD and PT-VWD have their characteristic symptoms, it is not easy to distinguish between them. Physicians follow a standardized flowchart to help them reach the correct diagnosis.⁵⁰ VWF levels and different VWD symptoms are measured and quantified. Since the diagnosis will influence the treatment, it is imperative to reach the correct conclusion. A misdiagnosis could be lethal. Patients with type PT-VWD present similar symptoms as type 2B VWD. Both subtypes exhibit low to normal platelet counts but maintain normal factor VIII and VIII-antigen activity.⁵⁰ They are sensitive to low concentrations of ristocetin, an activator, to induce platelet agglutination and have decreased high molecular weights of VWF multimers.⁵⁰ Therefore, it is crucial to accurately pinpoint the source of mutation. Ristocetin-induced platelet aggregation (RIPA) mixed studies and genetic testing⁵⁰ are two current ways physicians can differentiate between the PT-VWD and type 2B.

1.4.1. Ristocetin-Induced Platelet Aggregation Mixed Studies

Ristocetin-induced platelet aggregation (RIPA) assays utilities the concept that type 2B VWD possesses a gain-of-function mutation on VWF to induce a higher affinity to GPIIb/IIIa. The patient's VWF is incubated with platelet-rich plasma from a healthy individual and treated with a low concentration of ristocetin. If the patient has type 2B VWD, the

sample will respond to ristocetin and induce platelet aggregation. If the patient has a fully functional VWF, then the level of ristocetin will not induce aggregation.⁵¹ This assay can also be mixed to experiment on the patient's platelets by incubating them with healthy VWF samples. If the patient's platelets demonstrate high levels of aggregation with low levels of ristocetin, it can be concluded that the patient has PT-VWD.⁵¹ Although RIPA mixed studies prove to be highly informative of the patient's gain-of-function mutation, the assay is highly unstandardized. Both platelet and VWF samples are obtained from healthy individuals and the quality of the plasma will differ from person to person. Additionally, the shelf life of platelets is only five days long, placing a short expiration date on the resource.

1.4.2. Genetic Testing

Genetic testing is another way to test for PT-VWD. Patients suspected of type 2B VWD are advised to receive genetic sequencing to screen for type 2B mutations. If they test positive for one of the mutations, they are diagnosed with type 2B. If they do not test positive for any of the mutations, then there is a high chance they have PT-VWD. A RIPA mixed study may further confirm this diagnostic.⁵¹ Due to the rarity of PT-VWD, only four mutations have been reported⁴⁷ and it is uncommon to screen for PT-VWD mutations. Despite its conclusive results, genetic testing for PT-VWD is not comprehensive due to its reliance on the exclusion of type 2B. The assay is also lengthy and expensive for most hospitals.

1.4.3. Issues

Platelet-type and type 2B von Willebrand disease both present gain-of-function mutations that enhance the binding affinity between von Willebrand factor and GPIIb α . The two subtype's similar phenotypical symptoms make a diagnosis difficult. Ristocetin-induced platelet aggregation mixed studies and genetic testing are two assays used to determine whether the gain-of-function mutation exists on VWF or GPIIb α . However, RIPA mixed

studies are unstandardized and genetic testing is expensive and lengthy. 15% of PT-VWD cases are estimated to be misdiagnosed.⁴⁶ The biggest obstacle to acquiring more information regarding the subtype is the rarity of cases and inaccessibility to plasma samples. This study tackled this problem by establishing a cell-based model for PT-VWD to optimize a diagnostic assay using flow cytometry.

Chapter 2. Materials and Methods

2.1. Experimental Overview

In this study, we hypothesized that we can mimic the effects of PT-VWD by expressing the mutated GPIb α protein on the surface of cells. After establishing a cell-based model, we developed a novel diagnostic assay for PT-VWD utilizing flow cytometry. We utilized a Chinese hamster ovary (CHO) cell line and decided to express the W230L mutation due to its greatest effect on GPIb α .

We first established a stable CHO cell line expressing high levels of wildtype GPIb α and GPIb α (W230L). The transfection was conducted with a stable CHO cell line expressing GPIb β and GPIX. The expression of GPIb α was confirmed with western blot and flow cytometry. The cells underwent cell sorting to select for those with high expression of GPIb α . Lastly, the conditions for flow cytometry was optimized.

2.2. Establishment of a Stable Cell Line

2.2.1. The Plasmid

The engineered plasmid had a pcDNA 3.1 vector that contained the coding sequence for human GPIb α . In addition, it possessed a FLAG tag with the amino acids DYKDDDDK for identification, a hygromycin resistance gene, and several target sites for restrictive enzymes such as SPEI, NheI, XhoI, and EcoRI.

2.2.2. Restriction Digestion

The plasmid was sent to Genescript to conduct the site-directed W230L mutagenesis. Once received, the identity of the plasmid was confirmed with the use of restriction enzymes. NheI-HF (Catalog #R3131S), XhoI (Catalog #R0146S), EcoR1 (Catalog #R0101S), and SPEI-HF (Catalog #R3133S) from BioLabs (New England) were used. 500ng of the plasmid was used with 10x CutSmart (BioLabs), 1 μ L of digestive enzymes, and nuclease-

free water up to a volume of 25 μ L. The sample was let rest in a 37°C incubator for 45 minutes and ran on a 0.7% agarose gel with a 6x 1kb ladder (BioLabs).

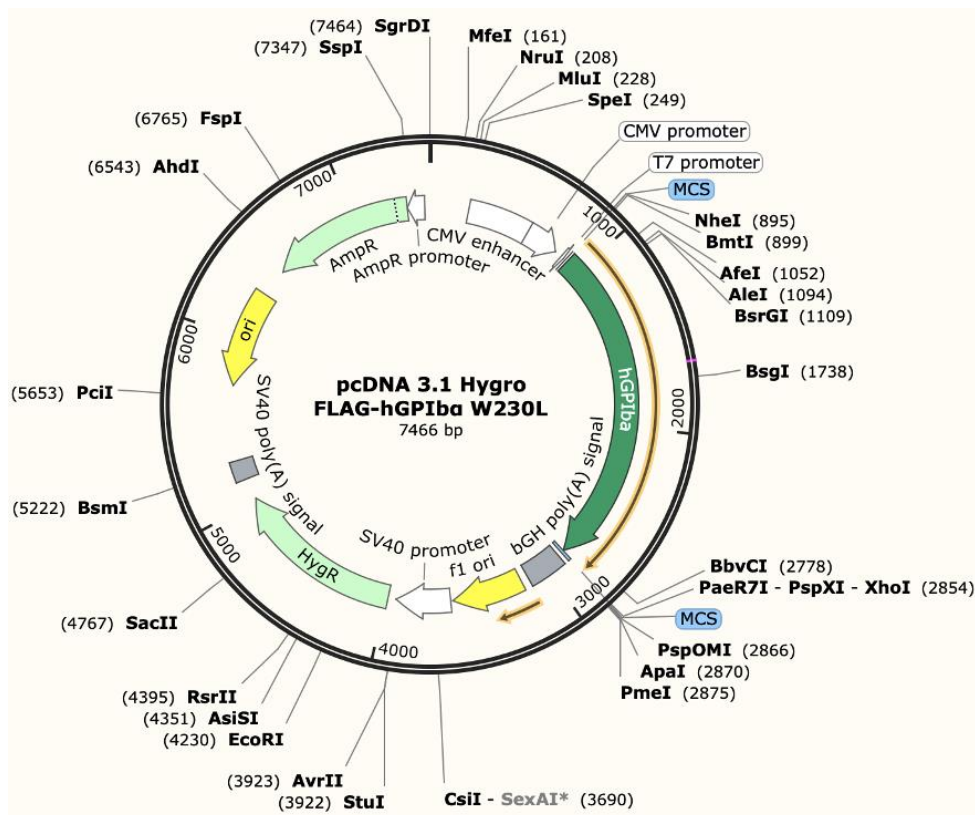


Figure 1. The Engineered GPIb α Plasmid. The plasmid contained the sequence for human GPIb α , an identification FLAG tag (DYKDDDDK), a hygromycin resistance gene, and several target sites for restrictive enzymes.

2.2.3. Cell Culture

Chinese hamster ovary cells (CHO) were grown in DMEM media with 10% fetal bovine serum (FBS) and 1% pen strep. At 80% confluency, the CHO cells were harvested or passed. 5 mL of Versene was added to the plate and placed in a 37°C incubator for 5 minutes. Once the cells have detached from the surface of the plate, they were harvested and centrifuged at 500 g for 5 minutes. The supernatant was removed and resuspended in PBS with 10% FBS and 0.01% sodium azide for experimental use. To pass the cells, the pellet was resuspended in 10 mL of DMEM and spread on a 10 cm cell culture plate.

2.2.4. Transfection

The transfection was performed with the lipofectamine 3000 transfection kit (Invitrogen, Waltham, MA. Catalog # L3000001) with a CHO cell line stably expressing GPIb α and GPIX. 2 μ l of lipofectamine and 2 μ L of P3000 were individually added to different tubes containing 75 μ L of Opti-MEM (Gibco, Waltham, MA. Catalog # [51985091](#)). 1 μ g of DNA was added to the lipofectamine solution and let rest for 5 minutes. The P3000 solution was combined with the lipofectamine solution, mixed gently, and let sit for 20 minutes. The solution was then added to a 12-well dish with CHO cells plated at 80% confluency in 1 mL of Opti-MEM. After 6 hours, the Opti-MEM was replaced with DMEM. The transfection was conducted for GPIb α (W230L), GPIb α WT, and GFP. An untransfected sample of CHO cells was also plated as a control.

2.2.5. Cell Lysis

48 hours after the transfection, the cells were harvested and 50 μ L of the cell lysis buffer (5mM N-Em, 58 mM sodium borate at pH 8.0, and 1% Triton-X 100) was added. Once the solution precipitated, the sample was spun down at 20,000 g for 15 minutes.

2.2.6. Western Blot

10 μ L of the cell lysis supernatant was used to check the cell's expression of GPIb α . The samples were boiled for 10 minutes and ran on an SDS page gel (GenScript) in reducing and non-reducing conditions. The 6x 1kb marker (BioLabs) was used as a reference and a sample of platelet lysate was run as a positive control. The antibodies used were WM23 and RAM1 that were produced and purified in the laboratory. The secondary antibodies were Goat anti-Mouse 680 RD (Li-COR, Lincoln, Nebraska. Catalog # 926-68070) and Goat anti-Rat 800 CW (Li-COR. Catalog # 926-32219).

2.2.7. Cell Sorting

A 10cm dish with confluent GPIb α (W230L) and GPIb α WT CHO cells were harvested and resuspended in 800 μ L of PBS with 10% FBS and 0.01% sodium azide. 50 μ L of PE anti-CD42a (BD Pharmingen, San Diego, California. Catalog #561853) and 10 μ L of APC anti-CD42b (BD Pharmingen, Catalog #551061) were added to the cells and incubated for 40 minutes on ice. The cells were centrifuged at 500g for 5 minutes and resuspended in 800 μ L of PBS with 10% FBS and 0.01% sodium azide. The solution was filtered with a 0.22 μ m membrane and added to 2 mL of DMEM. Flow cytometry with the BD FACSDiva software was used to sort for CHO cells expressing both GPIb α and GPIX at a high expression with APC and PE intensities from 10^3 - 10^4 . The remaining cells were grown in a 6-well dish and pressured with 250 μ g/mL of hygromycin (Invitrogen) and transferred to a 10 cm dish after confluency.

2.3. Flow Cytometry

GPIb α (W230L) and GPIb α WT were harvested at confluency in a 6-well dish and resuspended in PBS with 10% FBS and 0.01% sodium azide at 10^6 cells per mL. The samples were incubated with antibodies, plasma, or activators in a 96-well round-bottom plate for 30 minutes on ice. 200 μ L of PBS with 10% FBS and 0.01% sodium azide was added to the wells after incubation and centrifuged at 500g for 5 minutes. The excess liquid was removed from the plate and the cells were resuspended in 200 μ L of PBS with 10% FBS and 0.01% sodium azide.

The flow cytometry experiments were conducted with the CytoFLEX Flow Cytometry (Beckman Coulter, Brea, California). The fluorophores were standardized to intensities of 10^3 utilizing CHO cells incubated with the corresponding fluorophore as a

control. The events were gated to particles with a forward side scatter and side-side scatter that is characteristic of live cells. 10,000 events were collected within this gate for analysis.

2.3.1. Expression of GPIb α and GPIX

To check the expression of GPIb α and GPIX, 200 μ L of the resuspended cells were incubated with 20 μ L of PE anti-human CD42a and 2 μ L of APC anti-DYKDDDDK tag (BioLegend, San Diego, CA. Catalog # 37307). The samples were incubated on ice for 45 minutes to 1 hour.

2.3.2. GPIb α Binding to Full-length VWF

100 μ L of cells were incubated with purified biotinylated VWF at 250 μ M. To test the binding of GPIb α with full-length VWF in the plasma, 100 μ L of cells were incubated with an equal volume of pooled normal plasma (George King Bio-Medical, Overland Park, Kansas. Catalog #0010-1). When the plasma was diluted, the volume of cells at 10^6 cells per 50 μ L and plasma were added in ratios of neat, 1:2, 1:4, 1:16, 1:32, and 1:64 to a total volume of 10 μ L. The samples were also treated with 2 μ M of botrocetin. 3 μ L of FITC-conjugated anti-human VWF (Emfret Analytics, Eibelstadt, Germany. Catalog #P150-1) and 1 μ L of APC anti-DYKDDDDK tag were added to the mix and let incubate for 30 minutes.

2.3.3. Activators

1D12 is an A1 activator previously characterized by Ph.D. candidate Nicholas Arce in the laboratory. 50 μ L of pooled normal plasma and 50 μ L of cells were combined with different concentrations of 1D12 at 2000nM, 500nM, 125nM, 31nM, and 7.45nM. 2 μ L of FITC-conjugated anti-human VWF was added and the sample was left on ice for 30 minutes.

When working with botrocetin, 50 μ L of cells were incubated with 5 μ L of biotinylated A1 (1238-1493) at 0.3mg/mL, 1:1000 dilution of PE-conjugated Streptavidin (BD Pharmingen. Catalog #554061), and 1:100 dilution of Pacific Blue anti-DYKDDDDK tag.

Different concentrations of botrocetin at 0.5 μM , 1 μM , and 2 μM were added to the sample and let rest on ice for 1 hour.

2.3.4. Data analysis on FlowJo

The raw experimental data from CytoFLEX Flow Cytometry were imported to the software FlowJo. The x- and y-axes of SSC-H against FSC-H were adjusted to a logarithmic scale. Cells cluttered at a high intensity were selected for further analysis (Figure 2A).

Aggregated cells were sorted out by converting plotting SSC-H against SSC-A and drawing a vertical line below the high density areas (Figure 2B). The graph was then converted to a histogram, adjusting the x-axis to the fluorophore of interest as PE, APC, FITC, or PB (Figure 2C). The intensities of the control samples should center around 10^3 . Intensity levels higher than 10^3 demonstrate a positive response. The higher the intensity levels, the higher the binding. All statistical numbers of the number of events and average fluorescent intensity were obtained through FlowJo.

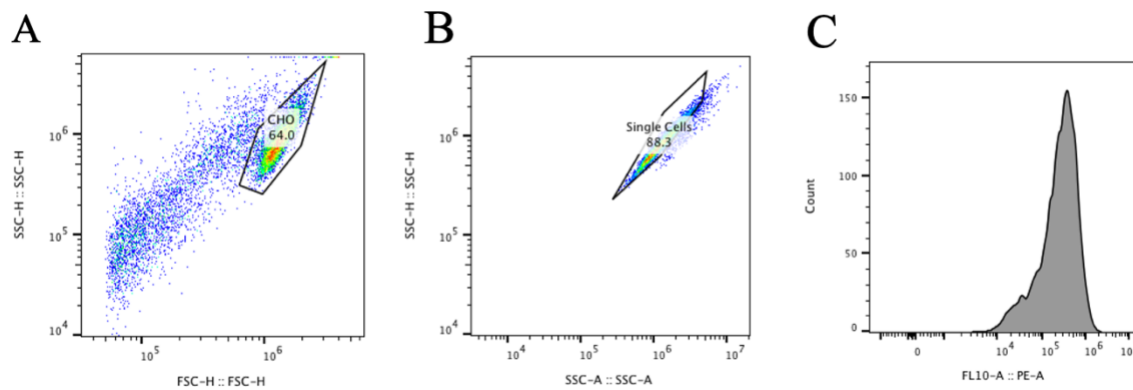


Figure 2. Event Selection for Data Analysis.

Chapter 3. Results and Discussion

3.1. Establishment of a Stable Cell Line

3.1.1. Confirmation of the Plasmid with Restriction Digestion

In this study, we established a cell-based model of platelet-type von Willebrand disease by expressing GPIb α on the surface of Chinese hamster ovary cells. The plasmid we engineered contained the sequence for human GPIb α , an identification FLAG tag (DYKDDDDK), a hygromycin resistance gene, and several target sites for restrictive enzymes such as SPEI, NheI, XhoI, and EcoRI. To confirm that the plasmid we received indeed contained the coding sequence for GPIb α , the plasmid was treated with three pairs of digestive enzymes. The samples treated with NheI and XhoI should yield two bands at 1959 and 5507 Da, EcoRI and SPEI at 3485 and 3981 Da, and XhoI at 7466 Da. The plasmid was confirmed to be correct after running the samples on an agarose gel.

3.1.2. Visualization of GFP in CHO cells

Previous research has demonstrated the necessity of expressing all three subunits of the GPIb-IX complex to ensure expression of GPIb α .⁴¹ Therefore, the transfection was performed with a CHO cell line stably expressing GPIb β and GPIX. The success of the transfection can be confirmed by running an SDS page gel of the cell lysis 48 hours after the procedure. After two unsuccessful attempts, it became useful to determine the success of the transfection without needing to undergo the two-day Western Blot experiment. As a result, green fluorescent protein (GFP) was transfected alongside the samples as a control. Cells that successfully integrated the plasmid into their DNA and expressed the protein would fluoresce green under the microscope. The GFP control samples provided an indirect way to determine the success of the transfection. Once GFP was visualized, the next step was initiated.

3.1.3. Validation of the GPIb α Transient Transfection by Western Blot

Forty-eight hours after transfection, the cells were harvested and lysed. The supernatants were run on an SDS page gel in reducing and non-reducing conditions. Platelet lysate was utilized as a positive control with its characteristic band at 135 kDa representing the alpha subunit of the glycoprotein Ib. Antibody WM23 was used to target GPIb α and RAM1 for GPIb β . The wild type and two W230L cell lines all exhibited a band at 135 kDa for GPIb α and 26 kDa for GPIb β . A higher band at around 200 kDa was also visualized on the western blot for the samples. It was hypothesized that this may be a combination of all

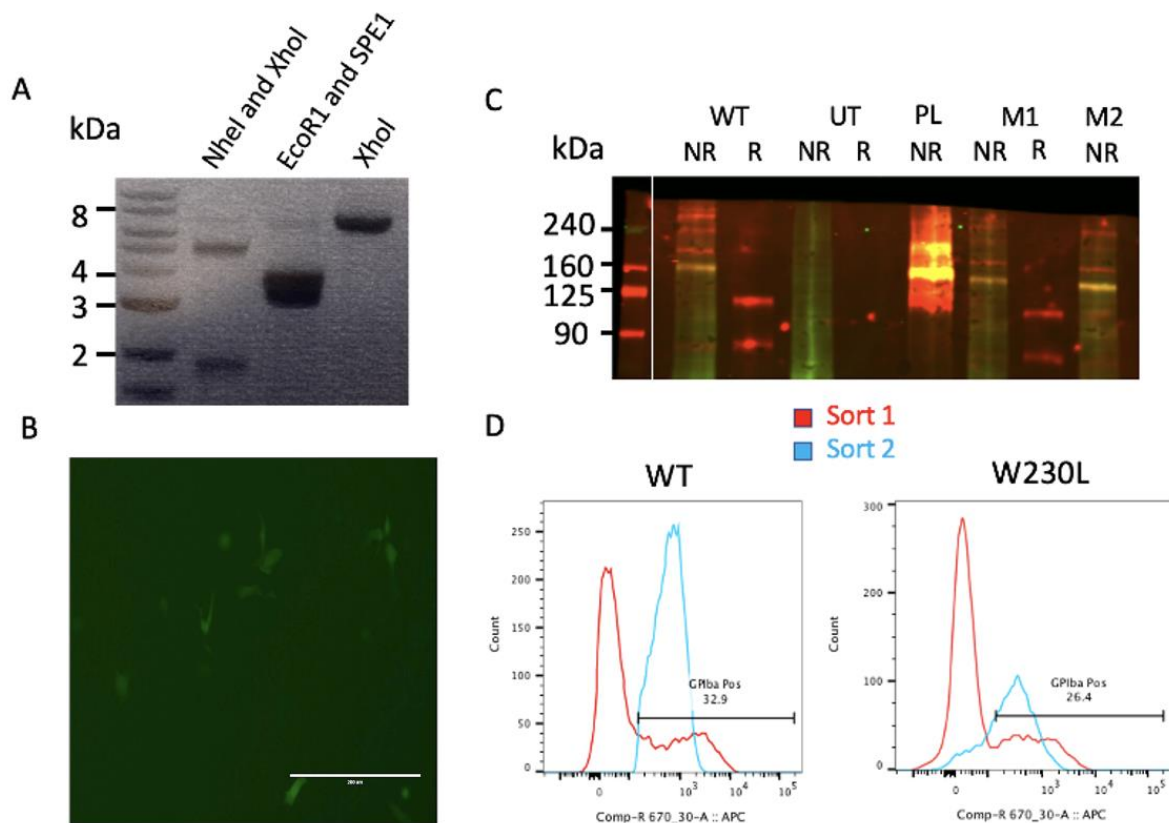


Figure 3. Establishment of a stable CHO cell line expressing GPIb α . (A) Agarose gel demonstrated the correct plasmid sizes of GPIb α after treated with restrictive enzymes. NheI and XhoI at 1959 and 5507 Da; EcoRI and SpeI at 3485 and 3981 Da; and XhoI at 7466Da. (B) Microscopic image of CHO cells fluoresced green 48 hours after transfection with GFP. (C) Western Blot with two GPIb α (W230L) samples demonstrated the presence of the alpha subunit at 135 kDa in non-reducing conditions. (D) Flow cytometry on the GPIb α (W230L) and GPIb α WT cell line after undergoing sorting. The second sort produced CHO cells with high expression levels of GPIb α in comparison to 32.9% and 26.4% of cells with high expression from the first sort.

three subunits of the glycoprotein with GPI β at 26 kDa and GPIX at 20 kDa; however, it is unclear what the bands may be exactly.

3.1.4. Enrichment of Cells Over-Expressing GPIb α by Flow Sorting

Once the expression of GPIb α was confirmed for the transient transfection of both GPIb α WT and GPIb α (W230L), the transfection was repeated with the optimized protocol. The cells were amplified and pressured with hygromycin, an antibiotic, to select for cells that are hygromycin resistant. The cell lines then underwent two sessions of cell sorting where those with high expression of both GPIb α and GPIX were kept. After amplification, the two cell lines were run on flow cytometry to determine their GPIb α and GPIX expression. Both GPIb α WT and GPIb α (W230L) demonstrated a low percentage of their cells with high fluorescence intensity of APC anti-TAG after the first sort. The population shifted drastically to the right after the second cell sort. A stable cell line of GPIb α (W230L) and GPIb α WT was established.

3.2. Higher Binding Affinity of GPIb α (W230L) with the von Willebrand Factor in Plasma

To determine whether the cell-based model of GPIb α (W230L) accurately reproduced the effects of platelet-type von Willebrand disease, the two cell lines were incubated with pooled normal plasma. Using flow cytometry, it was observed that the fluorescence intensity of FITC anti-VWF was shifted to the right for GPIb α (W230L) in comparison to GPIb α WT. The discrepancy between the two cell lines was minimum; however, this demonstrated the usability of the GPIb α (W230L) cell-based model.

3.3. Optimizing the Conditions

3.3.1. GPIb α (W230L) Responds Dose-Dependently to Botrocetin

Botrocetin, a snake venom, is known to activate VWF.⁵² The addition of botrocetin was hypothesized to increase the binding between GPIb α and the A1 domain. When the cells lines were incubated with pooled normal plasma and botrocetin at a concentration of 1 μ M and 2 μ M, the fluorescence intensities of both GPIb α (W230L) and GPIb α WT were shifted to the right in a dose-dependent manner; however, this shift was much more substantial for GPIb α (W230L). It was observed that GPIb α (W230L) exhibited a higher binding to VWF than its wild-type counterpart both with and without the presence of botrocetin. The binding

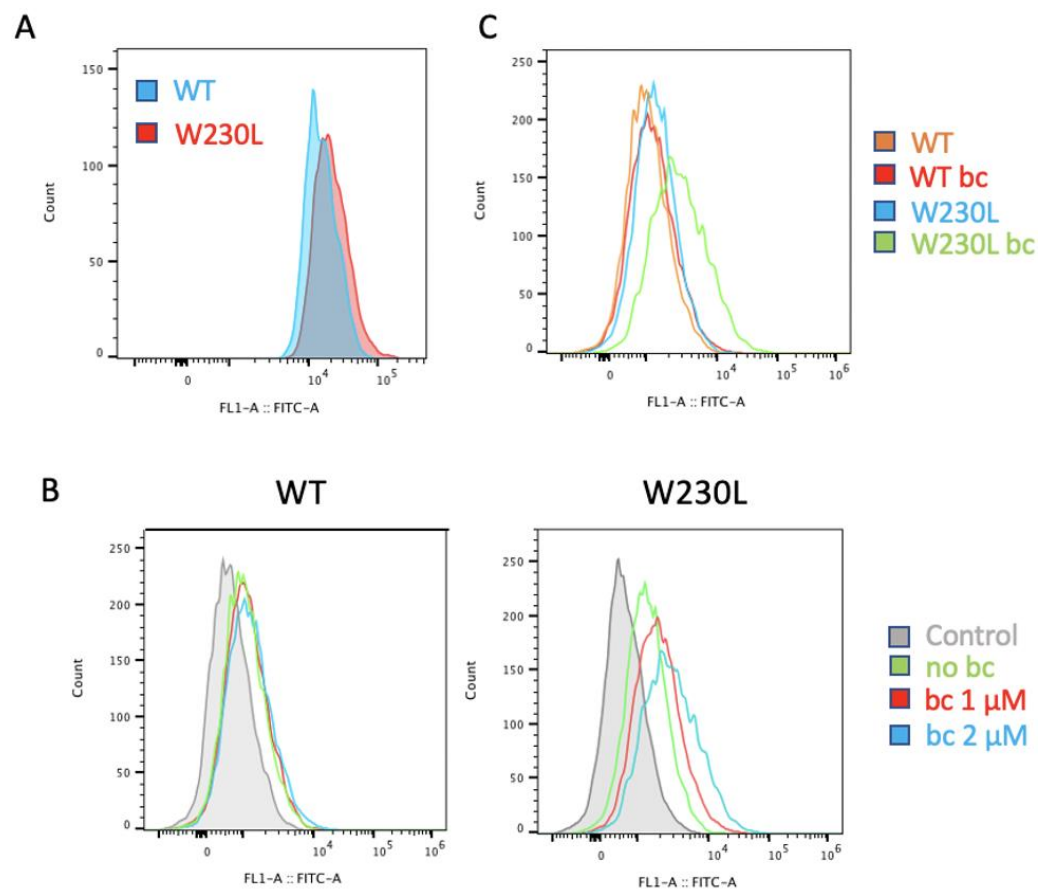


Figure 4. GPIb α (W230L) demonstrated higher binding to VWF in plasma than GPIb α WT in the presence of botrocetin. The binding of GPIb α WT with VWF in plasma did not change with the addition of botrocetin (bc). GPIb α (W230L) exhibited dose-dependent binding to VWF in plasma with botrocetin. Without botrocetin, GPIb α (W230L) exhibited slightly higher binding to VWF than GPIb α WT. However, this difference increased in the presence of 2 μ M of botrocetin.

of GPIb α (W230L) to VWF without botrocetin remained higher than the wild type's binding in the presence of botrocetin. As a result, GPIb α WT's lack of effect in a dose-dependent manner to botrocetin may magnify the binding differences between the two cell lines when a higher concentration of activator is used.

3.3.2. GPIb α (W230L) Exhibits Higher Binding to Activated A1

When the end region is removed from A1, the domain displays an enhanced binding ability to GPIb α and is "activated". The two cell lines were incubated with activated A1 at 900 nM for 30 minutes. Through flow cytometry, it was observed that GPIb α (W230L) exhibited higher binding to activated A1 than GPIb α WT. However, it was uncertain whether the difference in binding had resulted from the GPIb α (W230L) mutation or activated A1. Thus, the two cell lines were incubated with different concentrations of activated A1 and A1. GPIb α (W230L) and GPIb α WT exhibited higher binding to activated A1 than A1, with the mutant reaching an almost three-fold binding increase at 1 μ M. All four samples responded in a dose-dependent manner to A1. The maximum binding occurred at 1 μ M for GPIb α (W230L).

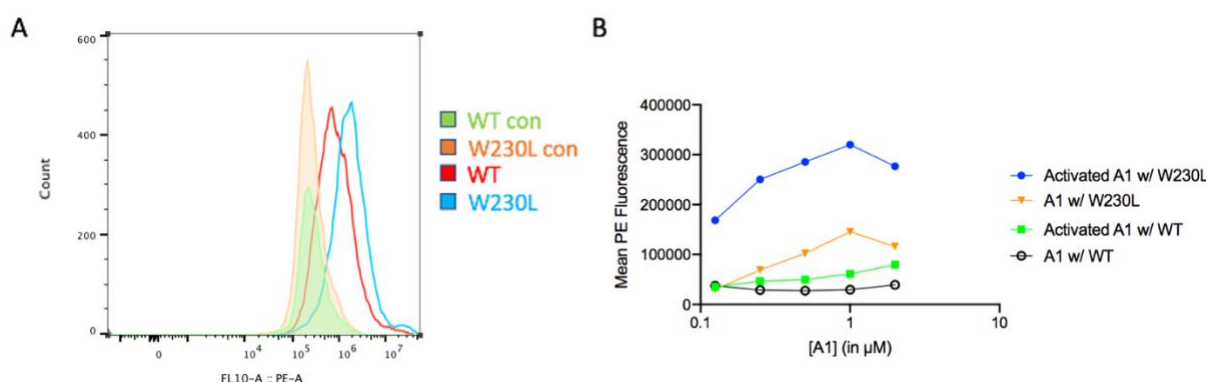


Figure 5. GPIb α (W230L) exhibited higher binding to activated A1 and bound in a dose-dependent manner with A1. (A) GPIb α (W230L) exhibited higher binding to activated A1 at 900 nM than GPIb α WT. (B) Both GPIb α (W230L) and GPIb α WT exhibited binding to activated A1 (1461) and A1 (1493) in a dose-dependent manner. A1 at 1 μ M produced the highest binding for GPIb α (W230L). The binding of GPIb α (W230L) with both activated A1 and A1 was significantly higher than GPIb α WT.

and was where the difference between the two cell lines was the greatest. Incubation of the wild type with activated A1 still resulted in a lower MFI than GPIb α (W230L) with A1.

3.3.3. Determining the Ideal Plasma Concentration at a 1:1 Dilution

We next explored the ideal plasma dilution to induce the highest binding response with GPIb α (W230L). In figure 5, we observed that although both cell lines responded to activated A1 and A1 in a dose-dependent manner, a concentration of 1 μ M provided the highest binding with GPIb α (W230L), not at 2 μ M as we might expect. A dilution not only alters the concentration of VWF but also the multitude of other proteins that exist in the plasma. Therefore, a dilution could potentially increase the accessibility of VWF by GPIb α . The plasma was incubated with the two cell lines at a ratio of neat, 1:1, 1:4, 1:6, 1:32, and 1:64. The average amount of VWF in plasma contains 1.8 to 1.9 international units per mL, where 1 IU/mL = 9.8 μ g/mL.⁵³ Neat plasma has a VWF concentration of approximately 69.7 μ M and this value was divided accordingly to obtain the different x-values. GPIb α (W230L)

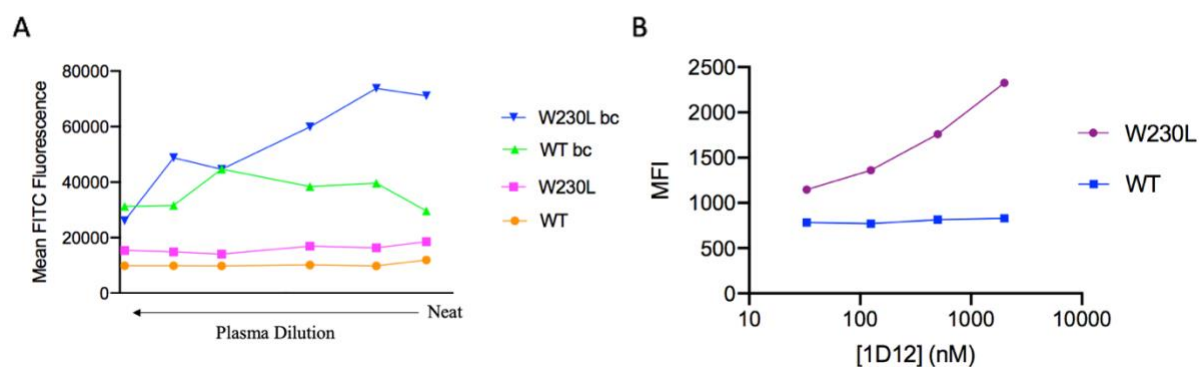


Figure 6. Diluting plasma at a 1:1 ratio and the addition of activators such as botrocetin and 1D12 increased the binding difference between GPIb α (W230L) and GPIb α WT.

(A) The mean FITC fluorescence intensity (MFI) was graphed against the plasma dilution. GPIb α (W230L) exhibited the highest MFI at a 1:1 ratio dilution of pooled plasma with PBS. The addition of botrocetin further increased the binding difference between GPIb α (W230L) and GPIb α WT. (B) The MFI was graphed against the concentration of 1D12 in nM. GPIb α (W230L) exhibited a dose-dependent binding to A1 in the presence of 1D12; however, the binding of the GPIb α WT remained consistent as the concentration of 1D12 increased.

and GPIb α WT that were not treated with botrocetin exhibited a consistent, minimum binding to VWF despite the increasing concentrations of VWF. On the other hand, the samples treated with botrocetin were observed to have a much higher MFI and responded in a dose-dependent manner. At a neat concentration of plasma, the MFI of both GPIb α (W230L) and GPIb α WT dropped compared to the 1:1 plasma dilution.

3.3.4. 1D12 is a Great Activator

1D12 was previously characterized by Ph.D. candidate Nicholas Arce as an activator of A1. GPIb α (W230L) and GPIb α WT were incubated with different concentrations of 1D12 at 2000 nM, 500 nM, 125 nM, and 31 nM in the presence of plasma diluted at a 1:1 ratio. It was observed that GPIb α (W230L) responded in a dose-dependent manner, with the highest binding at 2000 nM of 1D12. The binding of GPIb α WT with VWF remained consistent across the different concentrations of 1D12.

Chapter 4. Discussion

4 Discussion

In this paper, we established a stable CHO cell line expressing GPIb α (W230L) that exhibited enhanced binding to VWF in plasma and purified monomeric A1 in comparison to GPIb α WT. The addition of A1 activators such as botrocetin and 1D12, and the use of plasma at a 1:1 dilution further increased the binding of GPIb α (W230L). With these established parameters, it was possible to distinguish the two cell lines from each other to identify the GPIb α (W230L) sample through flow cytometry.

4.1. Optimizing the Use of Streptavidin-Conjugated Violet Fluorophore Beads

The assays in this paper utilized PE-conjugated streptavidin. However, we had attempted to optimize the use of streptavidin-conjugated violet fluorophore beads instead. A1 and activated A1 are not inherently fluorescent. Therefore, it was necessary to add a fluorophore to the incubation step to visualize the binding between GPIb α and A1. It was hypothesized that fluorescent A1 can be created by conjugating the protein to beads. Violet-fluorescent beads were selected due to the violet channel's lack of wavelength emission overlap with the FITC, APC, and PE channels on flow cytometry. The streptavidin-coated fluorescent purple beads were incubated with biotinylated A1 on a shaker at 1 hour, overnight, and for three days. After the conjugation, the beads were added to an equal volume of CHO cells and let rest for an hour.

When GPIb α (W230L) and GPIb α WT were incubated with the violet beads conjugated to A1 for an hour, two distinct peaks were detected despite gating for events that were pacific blue (anti-FLAG) positive. It was observed from a preliminary flow cytometry experiment that the streptavidin-conjugated violet beads have a characteristic violet 610 fluorescent intensity at around 10^5 . Therefore, the events with a fluorescent intensity around so were presumed to be CHO cells that have successfully bound to the bead-A1 complex. The other bigger peak represented cells that were not successful in doing so. Instead of

having a peak shifted towards the right, GPIb α (W230L) exhibited a higher number of events containing the fluorescent complex than GPIb α WT. Due to the low percentage of desired events at an hour incubation time, a longer 1 and 3-day conjugation time was tested, and GPIb α (W230L) was observed to have a significantly higher number of desired events at 3 days. However, the disparity between the two peaks remained overwhelming.

A control assay was run to determine the non-specific binding of the violet beads. GPIb α (W230L) and GPIb α WT were incubated with 3-day conjugated beads and beads that were not conjugated. Unexpectedly, the samples containing the unconjugated beads were

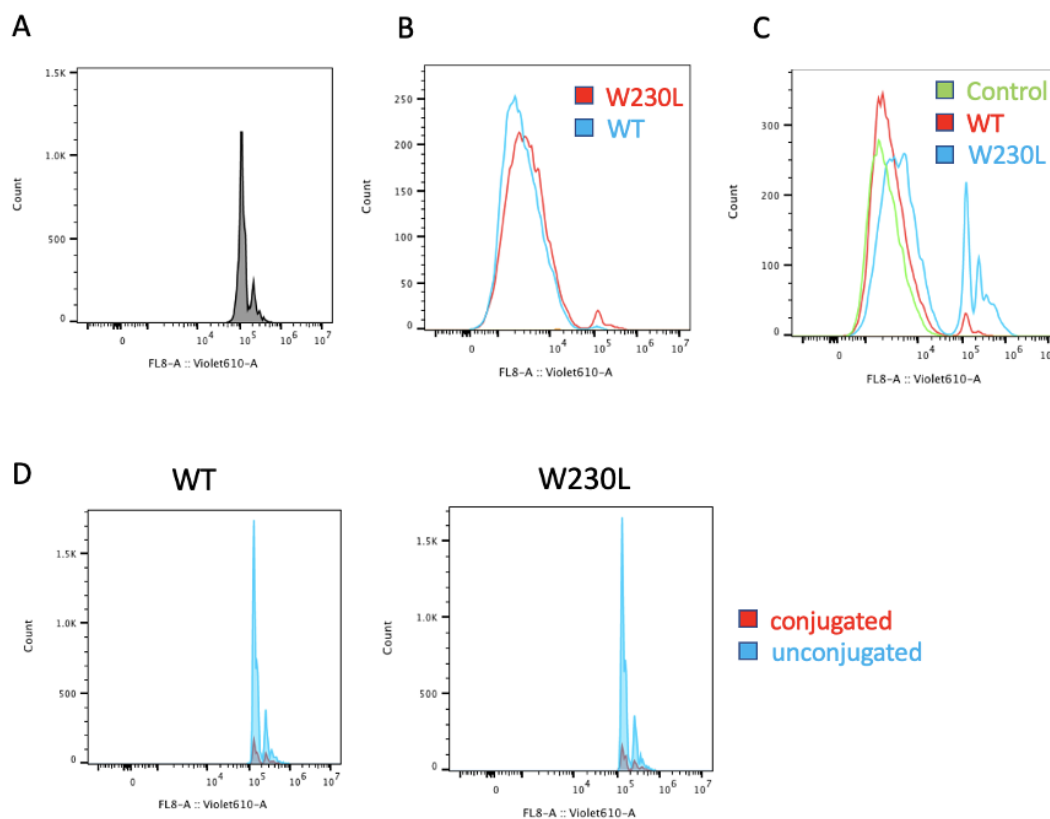


Figure 7. Non-specific binding of streptavidin-conjugated violet fluorophore beads with the GPIb α cell line. (A) The fluorescence intensity of the strep-conjugated violet fluorophore beads in the violet 610 channel has a characteristic intensity of 10⁵. (B) When the streptavidin-conjugated violet fluorophore beads was incubated with A1 for an hour, GPIb α (W230L) demonstrated slightly higher binding than GPIb α WT. (C) When the streptavidin-conjugated violet fluorophore beads were incubated with A1 overnight, the difference in binding of GPIb α (W230L) than GPIb α WT increased significantly. (D) Streptavidin-conjugated violet fluorophore beads without A1 demonstrated high, non-specific binding to both GPIb α WT and GPIb α (W230L).

observed to have a much higher number of pacific blue positive events than those with A1-conjugated beads. The significant amount of non-specific binding and difficulty working with the violet fluorescent beads had led to the decision to utilize PE-conjugated fluorophore instead. Luckily, both A1 and NAIM-A1 were biotinylated and can be identified with streptavidin fluorophores.

4.2. Further Studies with Ristocetin

A1 activators 1D12 and botrocetin have demonstrated their ability to increase the binding of GPIb α (W230L) and magnify the difference between the wild type and mutant samples. Future PT-VWD diagnostic assays may most likely require the use of some sort of activator to identify the mutation. However, both 1D12 and botrocetin were expressed and purified in this lab, rendering the acquisition of the activators more labor-intensive. Due to the laboratory shortage of ristocetin, the more accessible activator was not examined. Future experiments should prioritize the investigation of the effects of ristocetin and GPIb α (W230L).

4.3. The Declining Homogeneity of the CHO cell line

After a few months of passage, the CHO cell line exhibited an increasingly heterogeneous cell population with varying expression levels of GPIb α . Previous research have demonstrated that the interaction of GPIb α with VWF induces the apoptosis pathway.⁵⁴ Therefore, freezing down early generations of the cell line had proven to be useful and additional cell sorting after a few months is necessary. In the meantime, it may be beneficial to add a fluorophore-conjugated anti-FLAG during incubation and gate for positive events to re-establish a homogenous population through the data analysis.

4.4. Conclusion

Platelet-type von Willebrand disease is a rare and often misdiagnosed disease. Current diagnostic assays include genetic sequencing and RIPA mixed studies, which are costly and not standardized. This study established the first cell-based PT-VWD model by generating a stable cell line expressing GPIb α (W230L). The model had been observed to mimic the effects of PT-VWD by exhibiting an increased affinity binding to VWF and A1. Furthermore, the PT-VWD model responds in a dose-dependent manner to A1 activators. Through this study, we have established an optimized flow cytometry protocol and conditions to generate a distinct GPIb α (W230L) signal, warranting its use as a PT-VWD diagnostic assay. Additional experiments with our cell-based PT-VWD model could provide information regarding the rare disease.

References

1. Zhou, Y.; Eng, E.; Nishida, N.; Lu, C.; Walz, T.; Springer, T., A pH-regulated dimeric bouquet in the structure of von Willebrand factor. *EMBO J* **2011**, *30* (19), 4098-4111. DOI: 10.1038/emboj.2011.297
2. Zhou, Y.; Eng, E.; Zhu, J.; Lu, C.; Walz, T.; Springer, T., Sequence and structure relationships within von Willebrand factor. *Blood* **2012**, *120* (2), 449-458. DOI: 10.1182/blood-2012-01-405134
3. Wagner, D., Cell biology of von Willebrand factor. *Annu Rev Cell* **1990**, *6*, 217-246. DOI: 10.1146/annurev.cb.06.110190.001245
4. Sadler, J., New concepts in von Willebrand disease. *Annu Rev Cell* **2005**, *56*, 173-191. DOI: 10.1146/annurev.med.56.082103.104713
5. Yee, A.; Kretz, C., Von Willebrand factor: form for function. *Semin Thromb Hemost* **2014**, *40* (1), 17-27. DOI: 10.1055/s-0033-1363155
6. Huizinga, E.; Tsuji, S.; Romijn, R.; Schiphorst, M.; Groot, P. d.; Sixma, J.; Gros, P., Structures of glycoprotein Iba α and its complex with von Willebrand factor A1 domain. *Science* **2002**, *297* (5584), 1176-1179. DOI: 10.1126/science.107355
7. Blenner, M.; Dong, X.; Springer, T., Structural basis of regulation of von Willebrand factor binding to glycoprotein Ib. *J Biol Chem* **2014**, *289* (9), 5565-5579. DOI: 10.1074/jbc.M113.511220
8. Dumas, J.; Kumar, R.; McDonagh, T.; Sullivan, F.; Stahl, M.; Somers, W.; Mosyak, L., Crystal structure of the wild-type von Willebrand factor A1-glycoprotein Iba α complex reveals conformation differences with a complex bearing von Willebrand disease mutations. *J Biol Chem* **2004**, *279* (22), 23327-23334. DOI: 10.1074/jbc.M401659200

9. Huizinga, E.; Plas, R. v. d.; Kroon, J.; Sixma, J.; Gros, P., Crystal structure of the A3 domain of human von Willebrand factor: implications for collagen binding. *Structure* **1997**, *5* (9), 1147-1156. DOI: 10.1016/s0969-2126(97)00266-9
10. Emsley, J.; Cruz, M.; Handin, R.; Liddington, R., Crystal structure of the von Willebrand Factor A1 domain and implications for the binding of platelet glycoprotein Ib. *J Biol Chem* **1998**, *273* (17), 10396-10401. DOI: 10.1074/jbc.273.17.10396
11. Zhang, Q.; Zhou, Y.; Zhang, C.; Zhang, X.; Lu, C.; Springer, T., Structural specializations of A2, a force-sensing domain in the ultralarge vascular protein von Willebrand factor. *Proc Natl Acad Sci USA* **2009**, *106* (23), 9226-9231. DOI: 10.1073/pnas.0903679106
12. Jakobi, A.; Mashaghi, A.; Tans, S.; Huizinga, E., Calcium modulates force sensing by the von Willebrand factor A2 domain. *Nature Communications* **2011**, *2*, 385. DOI: 10.1038/ncomms1385
13. Zhou, M.; Dong, X.; Baldauf, C.; Chen, H.; Zhou, Y.; Springer, T. A.; Luo, X.; Zhong, C.; Gräter, F.; Ding, J., A novel calcium-binding site of von Willebrand factor A2 domain regulates its cleavage by ADAMTS13. *Blood* **2011**, *117* (17), 4623-4631. DOI: 10.1182/blood-2010-11-321596
14. Brondijk, T. H. C.; Bihan, D.; Farndale, R. W.; Huizinga, E. G., Implications for collagen I chain registry from the structure of the collagen von Willebrand factor A3 domain complex. *Proc Natl Acad Sci USA* **2012**, *109* (14), 5253-5258. DOI: 10.1073/pnas.1112388109
15. Huizinga, E. G.; Plas, R. M. v. d.; Kroon, J.; Sixma, J. J.; Gros, P., Crystal structure of the A3 domain of human von Willebrand factor: implications for collagen binding. *Structure* **1997**, *5* (9), 1147-1156.

16. Bienkowska, J.; M Cruz, A. A.; Handin, R.; Liddington, R., The von Willebrand factor A3 domain does not contain a metal ion-dependent adhesion site motif. *J Biol Chem* **1997**, 272 (40), 25162-25167. DOI: 10.1074/jbc.272.40.25162
17. Huang, R.-H.; Ying Wang, R. R.; Yu, X.; Purvis, A. R.; Heuser, J. E.; Egelman, E. H.; Sadler, J. E., Assembly of Weibel-Palade body-like tubules from N-terminal domains of von Willebrand factor. *Proc Natl Acad Sci USA* **2008**, 105 (2), 482-487. DOI: 10.1073/pnas.0710079105
18. Springer, T., von Willebrand factor, Jedi knight of the bloodstream. *Blood* **2014**, 124 (9), 1412-1425. DOI: 10.1182/blood-2014-05-378638
19. Luca, M. D.; Facey, D. A.; Favaloro, E. J.; Hertzberg, M. S.; Whisstock, J. C.; McNally, T.; Andrews, R. K.; Berndt, M. C., Structure and function of the von Willebrand factor A1 domain: analysis with monoclonal antibodies reveals distinct binding sites involved in recognition of the platelet membrane glycoprotein Ib-IX-V complex and ristocetin-dependent activation. *Blood* **2000**, 95 (1), 164-172.
20. Flood, V. H.; Friedman, K. D.; Gill, J. C.; Morateck, P. A.; Wren, J. S.; Scott, J. P.; Montgomery, R. R., Limitations of the ristocetin cofactor assay in measurement of von Willebrand factor function. *J Thromb* **2009**, 7 (11), 1832-1839. DOI: 10.1111/j.1538-7836.2009.03594.x
21. Flood, V. H.; Gill, J. C.; Morateck, P. A.; Christopherson, P. A.; Friedman, K. D.; Haberichter, S. L.; Branchford, B. R.; Hoffmann, R. G.; Abshire, T. C.; Paola, J. A. D.; Hoots, W. K.; Leissing, C.; Lusher, J. M.; Ragni, M. V.; Shapiro, A. D.; Montgomery, R. R., Common VWF exon 28 polymorphisms in African Americans affecting the VWF activity assay by ristocetin cofactor. *Blood* **2010**, 116 (2), 280-286. DOI: 10.1182/blood-2009-10-249102

22. Dong, J.-f.; Moake, J. L.; Nolasco, L.; Bernardo, A.; Arceneaux, W.; Shrimpton, C. N.; Schade, A. J.; McIntire, L. V.; Fujikawa, K.; López, J. A., ADAMTS-13 rapidly cleaves newly secreted ultralarge von Willebrand factor multimers on the endothelial surface under flowing conditions. *Blood* **2002**, *100* (12), 4033-4039. DOI: 10.1182/blood-2002-05-1401
23. Savage, B.; Sixma, J. J.; Ruggeri, Z. M., Functional self-association of von Willebrand factor during platelet adhesion under flow. *Proc Natl Acad Sci USA* **2002**, *99* (1), 425-430. DOI: 10.1073/pnas.012459599
24. Ulrichs, H.; Vanhoorelbeke, K.; Girma, J. P.; Lenting, P. J.; Vauterin, S.; Deckmyn, H., The von Willebrand factor self-association is modulated by a multiple domain interaction. *J Thromb Haemost* **2005**, *3* (3), 552-561. DOI: 10.1111/j.1538-7836.2005.01209.x
25. Fowler, W. E.; Fretto, L. J.; Hamilton, K. K.; Erickson, H. P.; McKee, P. A., Substructure of human von Willebrand factor. *J Clin Invest* **1985**, *76* (4), 1491-1500. DOI: 10.1172/JCI112129
26. Siedlecki, C. A.; Lestini, B. J.; Kottke-Marchant, K. K.; Eppell, S. J.; Wilson, D. L.; Marchant, R. E., Shear-dependent changes in the three-dimensional structure of human von Willebrand factor. *Blood* **1996**, *88* (8), 2939-2950.
27. Arce, N. A.; Cao, W.; Brown, A. K.; Legan, E. R.; Wilson, M. S.; Xu, E.-R.; Berndt, M. C.; Emsley, J.; Zhang, X. F.; Li, R., Activation of von Willebrand factor via mechanical unfolding of its discontinuous autoinhibitory module. *Nat Commun* **2021**, *12* (1), 2360. DOI: 10.1038/s41467-021-22634-x
28. Schneider, S. W.; Nuschele, S.; Wixforth, A.; Gorzelanny, C.; Alexander-Katz, A.; Netz, R. R.; Schneider, M. F., Shear-induced unfolding triggers adhesion of von Willebrand

factor fibers. *Proc Natl Acad Sci USA* **2007**, *104* (19), 7899-7903. DOI:

10.1073/pnas.0608422104

29. Ruggeri, Z. M.; Mendolicchio, G. L., Adhesion mechanisms in platelet function. *Circ Res* **2007**, *100* (12), 1673-1685. DOI: 10.1161/01.RES.0000267878.97021.ab

30. Savage, B.; Saldívar, E.; Ruggeri, Z. M., Initiation of platelet adhesion by arrest onto fibrinogen or translocation on von Willebrand factor. *Cell* **1996**, *84* (2), 289-297. DOI:

10.1016/s0092-8674(00)80983-6

31. Savage, B.; Almus-Jacobs, F.; Ruggeri, Z. M., Specific synergy of multiple substrate-receptor interactions in platelet thrombus formation under flow. *Cell* **1998**, *94* (5), 657-666.

DOI: 10.1016/s0092-8674(00)81607-4

32. Sing, C. E.; Alexander-Katz, A., Elongational flow induces the unfolding of von Willebrand factor at physiological flow rates. *Biophys* **2010**, *98* (9), L35-L37. DOI:

10.1016/j.bpj.2010.01.032

33. Ruggeri, Z. M.; Orje, J. N.; Habermann, R.; Federici, A. B.; Reininger, A. J., Activation-independent platelet adhesion and aggregation under elevated shear stress. *Blood* **2006**, *108* (6), 1903-1910. DOI: 10.1182/blood-2006-04-011551

34. Springer, T., Biology and physics of von Willebrand factor concatamers. *J Thromb Haemost* **2011**, *9*, 130-143. DOI: 10.1111/j.1538-7836.2011.04320.x

35. CDC Von Willebrand Disease (VWD). <https://www.cdc.gov/ncbddd/vwd/facts.html>.

36. Ruggeri, Z. M.; Pareti, F. I.; Mannucci, P. M.; Ciavarella, N.; Zimmerman, T. S., Heightened interaction between platelets and factor VIII/von Willebrand factor in a new subtype of von Willebrand's disease. *N Engl J Med* **1980**, *302* (19), 1047-1051. DOI:

10.1056/NEJM198005083021902

37. Quach, M. E.; Li, R., Structure-function of platelet glycoprotein Ib-IX. *J Thromb Haemost* **2020**, *18* (12), 3131-3141. DOI: 10.1111/jth.15035

38. McEwan, P. Y., W; Carr, K; Mo, X; Zheng, X; Li, R; Emsley, J, Quaternary organization of GPIb-IX complex and insights into Bernard-Soulier syndrome revealed by the structures of GPIb β and a GPIb β /GPIX chimera. *Blood* **2011**, *118* (19), 5292-5301. DOI: 10.1182/blood-2011-05-356253
39. Zarpellon, A.; Celikel, R.; Roberts, J. R.; McClintock, R. A.; Mendolicchio, G. L.; Moore, K. L.; Jing, H.; Varughese, K. I.; Ruggeri, Z. M., Binding of α -thrombin to surface-anchored platelet glycoprotein Ib(α) sulfotyrosines through a two-site mechanism involving exosite I. *Proc Natl Acad Sci USA* **2011**, *108* (21), 8628-8623. DOI: 10.1073/pnas.1017042108
40. Zhang, W.; Deng, W.; Zhou, L.; Xu, Y.; Yang, W.; Liang, X.; Wang, Y.; Kulman, J. D.; Zhang, X. F.; Li, R., Identification of a juxtamembrane mechanosensitive domain in the platelet mechanosensor glycoprotein Ib-IX complex. *Blood* **2015**, *125* (3), 562-569. DOI: 10.1182/blood-2014-07-589507
41. Mo, X.; Luo, S.-Z.; Munday, A. D.; Sun, W.; Berndt, M. C.; López, J. A.; Dong, J.-F.; Li, R., The membrane-proximal intermolecular disulfide bonds in glycoprotein Ib influence receptor binding to von Willebrand factor. *J Thromb Haemost* **2008**, *6* (10), 1789-1795. DOI: 10.1111/j.1538-7836.2008.03088.x
42. Miller, J. L.; Castella, A., Platelet-type von Willebrand's disease: characterization of a new bleeding disorder. *Blood* **1982**, *60* (3), 790-794.
43. Takahashi, H.; Sakuragawa, N.; Shibata, A., Von Willebrand disease with an increased ristocetin-induced platelet aggregation and a qualitative abnormality of the factor VIII protein. *Am J Hematol* **1980**, *8* (3), 299-308. DOI: 10.1002/ajh.2830080308
44. Casari, C.; Du, V.; Wu, Y.-P.; Kauskot, A.; Groot, P. G. d.; Christophe, O. D.; Denis, C. V.; Laat, B. d.; Lenting, P. J., Accelerated uptake of VWF/platelet complexes in

macrophages contributes to VWD type 2B-associated thrombocytopenia. *Blood* **2013**, *122* (16), 2893-2902. DOI: 10.1182/blood-2013-03-493312

45. Grover, N.; Boama, V.; Chou, M. R., Pseudo (Platelet-type) von Willebrand disease in pregnancy: a case report. *BMC Pregnancy and Childbirth* **2013**, *13* (16). DOI: 10.1186/1471-2393-13-16

46. Othman, M.; Kaur, H.; Favaloro, E. J.; Lillicrap, D.; Paola, J. D.; Harrison, P.; Gresele, P.; Physiology, S. o. v. W. D. a. P., Platelet type von Willebrand disease and registry report: communication from the SSC of the ISTH. *J Thromb Haemost* **2016**, *14* (2), 411-414. DOI: 10.1111/jth.13204

47. Tischer, A.; Machha, V. R.; Moon-Tasson, L.; Auton, M., Platelet-type von Willebrand disease: Local disorder of the platelet GPIIb/IIIa β -switch drives high-affinity binding to von Willebrand factor. *J Thromb Haemost* **2019**, *17* (12), 2022-2034. DOI: 10.1111/jth.14597

48. Othman, M.; Kaur, H.; Emsley, J., Platelet-type von Willebrand disease: new insights into the molecular pathophysiology of a unique platelet defect. *Semin Thromb Hemost* **2013**, *39* (6), 663-673. DOI: 10.1055/s-0033-1353442

49. Bury, L.; Falcinelli, E.; Bhotla, H. K.; Mezzasoma, A. M.; Guglielmini, G.; Tischer, A.; Moon-Tasson, L.; Auton, M.; Gresele, P., A p.Arg127Gln variant in GPIIb/IIIa LRR5 allosterically enhances affinity for VWF: a novel form of platelet-type VWD. *Blood Adv* **2021**, *bloodadvances*.

50. James, P. D.; Connell, N. T.; Ameer, B.; Paola, J. D.; Eikenboom, J.; Giraud, N.; Haberichter, S.; Jacobs-Pratt, V.; Konkle, B.; McLintock, C.; McRae, S.; Montgomery, R. R.; O'Donnell, J. S.; Scappe, N.; Robert Sidonio, J.; Flood, V. H.; Husainat, N.; Kalot, M. A.; Mustafa, R. A., ASH ISTH NHF WFH 2021 guidelines on the diagnosis of von

Willebrand disease. *Blood Advances* **2021**, 5 (1), 280-300. DOI:

10.1182/bloodadvances.2020003265

51. Frontroth, J. P.; Favaloro, E. J., Ristocetin-Induced Platelet Aggregation (RIPA) and RIPA Mixing Studies. *Methods Mol Biol* **2017**, 1646, 473-494. DOI: 10.1007/978-1-4939-7196-1_35

52. Matsui, T.; Hamako, J., Structure and function of snake venom toxins interacting with human von Willebrand factor. *Toxicon* **2005**, 45 (8), 1075-1087. DOI: 10.1016/j.toxicon.2005.02.023

53. ab108918 Human Von Willebrand Factor (VWF) ELISA Kit. Abcam: 2018; p 17.

54. Li, S.; Wang, Z.; Liao, Y.; Zhang, W.; Shi, Q.; Yan, R.; Ruan, C.; Dai, K., The glycoprotein Ib α -von Willebrand factor interaction induces platelet apoptosis. *Journal of Thrombosis and Haemostasis* **2009**, 8 (2), 341-50. DOI: 10.1111/j.1538-7836.2009.03653.x